Output-Feedback Controller Design for a Sun-Tracking Photovoltaic Device

Teal Hobson-Lowther
Colorado School Of Mines, *Dept. of Electrical Engineering and Computer Science*

I. Introduction

In this paper, I set out to control the face angles of a solar panel via DC motors. The hope is to consistently and reliably achieve the maximum power output of a particular panel, increasing its overall efficiency.

The maximum power output of a solar panel is generated when the panel face is perpendicular to the vector pointing from the panel to the sun. Because of the dynamic nature of the sun's position in the sky, stationary solar panels are unable to consistently capture the maximum solar energy throughout the day. Traditionally, this problem is "solved" with a blanket method of placing a panel in a permanent orientation such that it generates the maximum average energy for fixed azimuthal and zenith angles [1].

Three alternative solutions are proposed that track pre-computed optimal solar angle set points (obtained from [2]). The first solution is a simplistic proof-of-concept model that uses reference-tracking output-feedback control with constant gain. The second is a more developed model that incorporates actuator saturation. The third incorporates both actuator saturation and gain-scheduling reference-tracking output-feedback control.

II. Control Goals

We wish to alter the solar panel's azimuthal and incident angles to conform to reference input angles. The position of the sun in the sky changes so slowly that settling time design requirements are less important than overshoot requirements. For all three designs, settling times of over 2 minutes for either angle are undesirable for reference update intervals of 30 minutes. Overshoot and steady-state errors of more than 5% are intolerable, and deviations past angles of $\pm\pi$ rad would be past the potentiometer's sensing range.

In the second model, a saturation of $\pm 12V$ is applied to the controller output voltages. This is a realistic non-linearity in motors with constant internal resistances and maximum current ratings.

The third model has the same constraint on the input. In addition, gain-scheduling is implemented on the output-feedback controller such that the gain is larger when the reference error is large. These two constraints introduce some interesting non-linear characteristics into the controller.

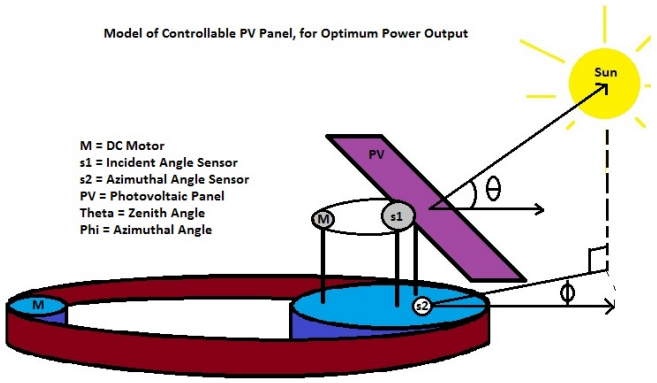

Figure 1: Model of a controllable PV angle. θ and ϕ angles of the solar panel will be compared to optimal angles provided by [2]. Motors M alter the two angles.

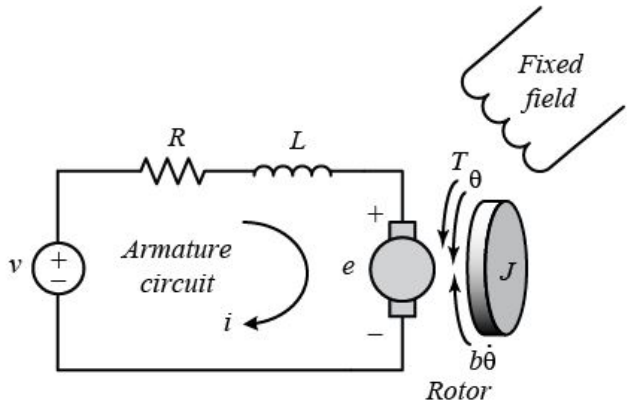

Figure 2: DC motor circuit, obtained from [5]. θ and ϕ will be controlled with identical, decoupled motors.

III. Modeling

To perform a simulation, I will take specifications from the SunModule SW 250 Mono solar panel and Eltrex Penta 1L motors. The specification sheets may be found in [3] and [4].

We consider the plant to be a combined motor and solar panel system (Figure 1), The outputs of the system are angles which correspond to the incident and azimuthal angles of the panel: θ and ϕ, respectively. The inputs are the control voltages sent to the motors that control each angle, V_θ and V_ϕ (Figure 2).

The state-space representation (6) is generated by finding the transfer functions between the voltage input to the motors and the angular positions of the panel, $\frac{\Theta(s)}{V_\theta(s)}$ and $\frac{\Phi(s)}{V_\phi(s)}$ (4,5), and then representing the system in control canonical form. For a complete derivation of each dynamical equation and transfer function, see [5].

The dynamical equations which govern the interaction of the motors and panel angles for both models are shown in (1), (2), and (3). The second and third model have an additional constraint (7) on the input voltages. For all variables, the subscripts θ and ϕ represent the variables pertaining to the incident and azimuthal angles, respectively. I_θ and I_ϕ represent the inertia of the solar panel, M the mass, w and l the width and length of the panel, b_θ and b_ϕ the motor viscous friction constants, K_θ and K_ϕ the motor torque constants, R_θ and R_ϕ the internal motor resistances, L_θ and L_ϕ the internal motor inductance, V_θ and V_ϕ the voltage applied to motor terminals, i_θ and i_ϕ the currents through each motor:

$$\mathrm{I}_\theta = \frac{Ml^2}{12} \qquad \mathrm{I}_\phi = \frac{M(l^2+w^2)}{12} \tag{1}$$

$$\mathrm{I}_\theta\ddot{\theta} + \mathrm{b}_\theta\dot{\theta} = \mathrm{K}_\theta i_\theta \qquad \mathrm{I}_\phi\ddot{\phi} + \mathrm{b}_\phi\dot{\phi} = \mathrm{K}_\phi i_\phi \tag{2}$$

$$\mathrm{L}_\theta\frac{di_\theta}{dt} + \mathrm{R}_\theta i_\theta = \mathrm{V}_\theta - \mathrm{K}_\theta\dot{\theta} \qquad \mathrm{L}_\phi\frac{di_\phi}{dt} + \mathrm{R}_\phi i_\phi = \mathrm{V}_\phi - \mathrm{K}_\phi\dot{\phi} \tag{3}$$

The equations above yield the following transfer functions:

$$\frac{\theta(s)}{\mathrm{V}_\theta} = \frac{\frac{\mathrm{K}_\theta}{\mathrm{I}_\theta\mathrm{L}_\theta}}{s^3 + \frac{\mathrm{I}_\theta\mathrm{R}_\theta + \mathrm{b}_\theta\mathrm{L}_\theta}{\mathrm{I}_\theta\mathrm{L}_\theta}s^2 + \frac{\mathrm{b}_\theta\mathrm{R}_\theta + \mathrm{K}_\theta{}^2}{\mathrm{I}_\theta\mathrm{L}_\theta}s} \tag{4}$$

$$\frac{\phi(s)}{\mathrm{V}_\phi} = \frac{\frac{\mathrm{K}_\phi}{\mathrm{I}_\phi\mathrm{L}_\phi}}{s^3 + \frac{\mathrm{I}_\phi\mathrm{R}_\phi + \mathrm{b}_\phi\mathrm{L}_\phi}{\mathrm{I}_\phi\mathrm{L}_\phi}s^2 + \frac{\mathrm{b}_\phi\mathrm{R}_\phi + \mathrm{K}_\phi{}^2}{\mathrm{I}_\phi\mathrm{L}_\phi}s} \tag{5}$$

Letting $\vec{x} = |x_1, x_2, x_3, x_4, x_5, x_6,|^T$, $\vec{u} = |V_\theta, V_\phi|^T$, and deriving the controller canonical form of each transfer function yields state space equation $\dot{\vec{x}} = \mathrm{A}\vec{x} + \mathrm{B}\vec{u}$, $\vec{y} = \mathrm{C}\vec{x} + \mathrm{D}\vec{u}$, with:

$$A = \begin{vmatrix} 0 & 1 & 0 & 0 & 0 & 0 \\ 0 & 0 & 1 & 0 & 0 & 0 \\ 0 & -\mathrm{a}_{\theta 1} & -\mathrm{a}_{\theta 2} & 0 & 0 & 0 \\ 0 & 0 & 0 & 0 & 1 & 0 \\ 0 & 0 & 0 & 0 & 0 & 1 \\ 0 & 0 & 0 & 0 & -\mathrm{a}_{\phi 1} & -\mathrm{a}_{\phi 2} \end{vmatrix}$$

$$B = \begin{vmatrix} 0 & 0 & 1 & 0 & 0 & 0 \\ 0 & 0 & 0 & 0 & 0 & 1 \end{vmatrix}^T \tag{6}$$

$$C = \begin{vmatrix} \frac{\mathrm{K}_\theta}{\mathrm{I}_\theta\mathrm{L}_\theta} & 0 & 0 & 0 & 0 & 0 \\ 0 & 0 & 0 & \frac{\mathrm{K}_\phi}{\mathrm{I}_\phi\mathrm{L}_\phi} & 0 & 0 \end{vmatrix} \qquad D = \begin{vmatrix} 0 & 0 \\ 0 & 0 \end{vmatrix}$$

$$u_{\theta,\phi} = \begin{cases} u_{\theta,\phi_{min}} & u_{\theta,\phi} < u_{\theta,\phi_{min}} \\ u_{\theta,\phi} & u_{\theta,\phi_{min}} < u_{\theta,\phi} < u_{\theta,\phi_{max}} \\ u_{\theta,\phi_{max}} & u_{\theta,\phi_{max}} < u_{\theta,\phi} \end{cases} \tag{7}$$

where $\mathrm{a}_{\alpha 1} = (\frac{\mathrm{b}_\alpha\mathrm{R}_\alpha + \mathrm{K}_\alpha{}^2}{\mathrm{I}_\alpha\mathrm{L}_\alpha})$ and $\mathrm{a}_{\alpha 2} = (\frac{\mathrm{I}_\alpha\mathrm{R}_\alpha + \mathrm{b}_\alpha\mathrm{L}_\alpha}{\mathrm{I}_\alpha\mathrm{L}_\alpha})$, $\alpha = \theta, \phi$.

IV. Analysis

A. Open-Loop Plant Stability

Because this open-loop system is completely linear, stability analysis equates to the determination of the eigenvalues of A.

To begin this analysis, first we notice that the A matrix described in (6) is a decoupled system. This means that the matrix A can be written in block matrix form as follows:

$$\mathrm{A} = \begin{vmatrix} \mathrm{A}_\theta & 0 \\ 0 & \mathrm{A}_\phi \end{vmatrix} \tag{8}$$

where

$$A_\alpha = \begin{vmatrix} 0 & 1 & 0 \\ 0 & 0 & 1 \\ 0 & -\mathrm{a}_{\alpha 1} & -\mathrm{a}_{\alpha 2} \end{vmatrix} \qquad \text{with } \alpha = \theta, \phi \tag{9}$$

Now, the eigenvalues of the matrix A are simply the eigenvalues of A_θ along with those of A_ϕ. These are found with the strategy of setting the determinant of the following matrices equal to 0:

$$\det(s\mathrm{I} - \mathrm{A}_\theta) = \det(s\mathrm{I} - \mathrm{A}_\phi) = 0 \tag{10}$$

Keep in mind that the values of $\mathrm{a}_{\theta 1}$, $\mathrm{a}_{\theta 2}$, $\mathrm{a}_{\phi 1}$, and $\mathrm{a}_{\phi 2}$ are strictly positive. To continue our analysis, we must find the determinants specified in (10). This yields the following pair of characteristic equations:

$$s_\theta[s_\theta(s_\theta + \mathrm{a}_{\theta 2}) + \mathrm{a}_{\theta 1}] = 0 \qquad s_\phi[s_\phi(s_\phi + \mathrm{a}_{\phi 2}) + \mathrm{a}_{\phi 1}] = 0 \tag{11}$$

Each equation clearly has a pole located at $s_{\theta 1} = s_{\phi 1} = 0$, indicating that they fall on the closed left half-plane (CLHP).

Some manipulation of the equations which remain after dividing each equation in (11) through by s_θ and s_ϕ, resp., yields the following quadratics:

$$s_\theta = \frac{-\mathrm{a}_{\theta 2} \pm \sqrt{{\mathrm{a}_{\theta 2}}^2 - 4\mathrm{a}_{\theta 1}}}{2} \qquad s_\phi = \frac{-\mathrm{a}_{\phi 2} \pm \sqrt{{\mathrm{a}_{\phi 2}}^2 - 4\mathrm{a}_{\phi 1}}}{2} \tag{12}$$

Extensive algebra on (12) will show that the remaining poles, $s_{\theta 2}, s_{\theta 3}, s_{\phi 2}$, and $s_{\phi 3}$ are all in the open left-half plane (OLHP) so long as the condition:

$$0 < \mathrm{a}_{\alpha 1} < \frac{{\mathrm{a}_{\alpha 2}}^2}{4} \tag{13}$$

is met. For the parameters of our simulation, this is met by about 3 orders of magnitude.

The result of this analysis shows that the open-loop system (6) has 2 poles located in the CLHP and 4 poles located in the OLHP. In general, a system that has repeated roots on the imaginary axis is **unstable**. Analysis of the controllability of this system will determine whether or not these poorly-behaved poles may be moved into the OLHP to yield an asymptotically stable system.

B. Controllability and Observability

Since we have two poles located on the CLHP, an analysis of the controllability and observability of this representation is imperative before we attempt to develop any kind of controller.

The controllability of this system is determined by the rank of the controllability matrix, CC, which in our case is 6. Because the rank of CC is equal to the dimension of our A matrix, **all poles are controllable** and therefore the open-loop system is **stabilizable**.

The observability of this system is determined by the rank of the observability matrix, O, which in our case is 6. Because the rank of O is equal to the dimension of our A matrix, **all poles are observable**, and therefore the open-loop system is **detectable**.

V. Design 1: Reference Tracking Output-Feedback Controller with Constant Gain

When considering what type of controller to implement, several factors came into play. Because the poles we wish to stabilize are found in the output of our system, it is unnecessary to implement a digital state estimator circuit into the controller design. Because the output angles of our system θ and ϕ can easily be fed into an electrical circuit which converts them into scaled voltages and compares to a reference voltage, an output-feedback controller was selected as the most obvious and affordable initial design. The general configuration for this system is shown in Figure 3.

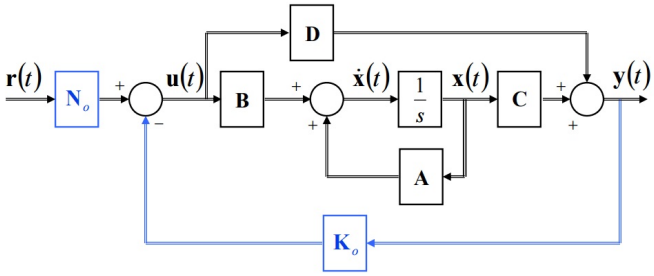

Figure 3: General form block-diagram for reference-tracking output-feedback control. The values of K_0, N_0 are determined experimentally. Figure obtained from [6].

A. Deriving K_0, N_0

The output-feedback gain matrix K_0 necessary to control our system will place poorly behaved poles which are associated with the output states into the OLHP. In our case, this equates to moving the poles at $s_{\theta 1}$ and $s_{\phi 1}$, which are located at 0. Adding an output feedback gain matrix changes the state space representation to the following form:

$$\dot{\vec{x}} = (A - BK_0)\vec{x} + BN_0\vec{r} \tag{14}$$

Moving the poles to a desired location involves finding a K_0 matrix such that the solutions to this equation always fall in the OHLP:

$$\det(s\mathrm{I} - A + BK_0) = 0 \tag{15}$$

Define the K_0 matrix to have arbitrary elements, to be determined in the following analysis:

$$K_0 = \begin{vmatrix} k_{11} & k_{12} \\ k_{21} & k_{22} \end{vmatrix} \tag{16}$$

After much algebra, it is seen that in our case (15) has no poles on the imaginary axis if and only if:

$$(k_{12}k_{21} - k_{11}k_{22}) \neq 0 \tag{17}$$

Because we are looking for the simplest and most affordable implementation of our controller, let us take $k_{12} = k_{21} = 0$. This makes the K_0 matrix diagonal, and further capitalizes on the separability of this system. After some experimentation, $k_{11} = 6$ and $k_{22} = 7$ are found to be suitable entries of K_0 which accomplish the design goals with our specific system parameters. Additionally, because it meets the requirements of (15), the

closed-loop system has all 6 poles in the OLHP, and the controlled system is now **asymptotically stable**.

$$K_0 = \begin{vmatrix} 6 & 0 \\ 0 & 7 \end{vmatrix} \tag{18}$$

What is K_0 in a physical sense? Essentially K_0 is a potentiometer circuit which takes as input the angles θ and ϕ and translates them into scaled voltages $V_{\theta k}$ and $V_{\phi k}$ through a voltage divider circuit. In other words, the elements of K_0 should have units of $\frac{V}{rad}$. Since the K_0 designed above is diagonal, we can make parallel circuits which run the outputs θ, ϕ through gains of values $6\frac{V}{rad}$ and $7\frac{V}{rad}$, corresponding to the values of k_{11} and k_{22}, respectively. We can then feed the voltages into a Wheatstone Bridge differential amplifier with unit gain, and this will give us an error voltage directly proportional to the difference of the reference angle voltages and the K_0 output voltages.

When we incorporate the output feedback matrix K_0 into this circuit, we must run the reference signals V_θ and V_ϕ through a matrix N_0 which makes the voltages output by N_0 proportional to the voltages output by K_0. This equates to putting gains of the same values as k_{11} and k_{22} into the diagonal entries:

$$N_0 = \begin{vmatrix} 6 & 0 \\ 0 & 7 \end{vmatrix} \tag{19}$$

B. Performance

1) Step Response: The response of the Design 1's closed-loop system to a pair of unit step reference inputs is shown in Figure 4. The initial angle errors shown are some of the more extreme one would expect to see in a real physical situation. As can be seen, after two minutes there is less than .001% overshoot in either state, and the steady-state error is less than 4.13% for θ and less than .0005% for ϕ. The control goals have been met by this output-feedback controller design.

2) Required Control Effort: The motors we have chosen for this model are rated for an input voltage magnitude of 0-48V. A plot of our simulated control voltage versus time is shown in Figure 5. Clearly, the control voltages fall safely within this rated range, with the control voltage to θ reaching its maximum at a magnitude of under 17.98V, and the control voltage of ϕ reaching its maximum at a magnitude of just under 21V. It seems safe to say that a larger disturbance would drive the error voltage to one higher than that which the motors are rated for. Most of the required effort evolves from high initial conditions on states $\dot{\theta}$ and $\dot{\phi}$.

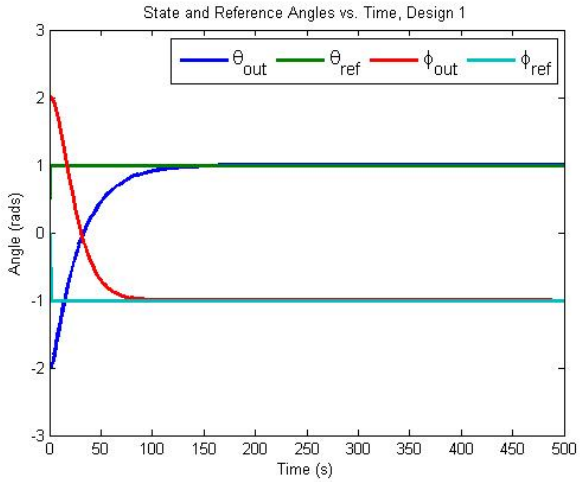

Figure 4: Response of plant outputs to unit-step input, Design 1.

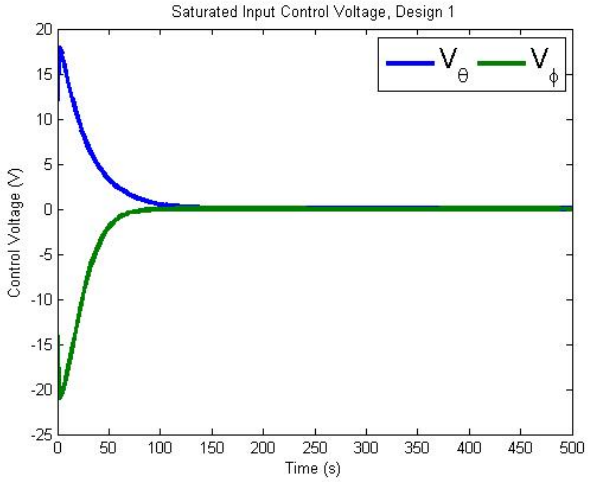

Figure 5: Plot of control voltage passed to the DC motors vs. time, Design 1.

VI. Design 2a: Reference Tracking Output-Feedback Controller with Constant Gain and Model Nonlinearities

Although the controller of the previous section was successful, there are certain nonlinearities in the solar panel control system to address. Placing a saturation (7) on the plant input voltage allows us to model power constraints on small motors.

A. Deriving K_0, N_0

For this simulation, the K_0 and N_0 matrices are the same as in (18) and (19).

B. Performance

1) Step Response: The results of placing a saturation on the plant input voltage are shown in Figure 6 and Figure 7. Figure 6 shows the reference angles and state output angles as a function of time. We can see that after two minutes the state error in θ is 4.5%, and the steady-state error in ϕ is .0006%, still meeting our original design requirements, although settling slower than Design 1. This is not a surprising result. The saturation in the motor voltages results in less torque application to the panel, and therefore a slower response time.

2) Required Controller Effort: In Figure 7 we can see the saturation on the inputs of the θ motor. We have now met the requirement that motor inputs stay between designated values of $\pm 12V$.

VII. Design 2b: Reference Tracking Output-Feedback Controller with Gain-Scheduling and Model Nonlinearities

The last design goal is a tracking system whose control effort is proportional to the size of the reference tracking error. We would like to correct large angle differences between the output and the reference input, but we don't care as much about small angle differences. The source of this idea comes from the physics of solar insolation, where small deviations from the optimal tracking angle are less damaging to solar efficiency [1], and thus not as imperative to correct.

A. Deriving K_0, N_0

In this model, it is more important to control for large angle errors. An attempt to reflect that decision in a gain-scheduled output-feedback controller, K, yields:

$$K = \begin{cases} .1K_{max} & |\theta_{ref} - \theta| < .3 \\ .5K_{max} & .3 \leq |\theta_{ref} - \theta| < 1 \\ K_{max} & 1 \leq |\theta_{ref} - \theta| \end{cases} \tag{20}$$

where K_{max} is set to be the same as K_0 in (18).

By the same reasoning as in the discussion of Design 1, the reference gain matrix N must now be scaled proportionally to K.

B. Performance

1) Step Response: The results of implementing a gain-scheduled controller on the non-linear plant are shown in Figure 8 and Figure 9. Figure 8 shows the reference and plant output angles as a function of time. The state error in θ after 2 minutes is 8.61%. The state error in ϕ after 2 minutes is 2.97%.

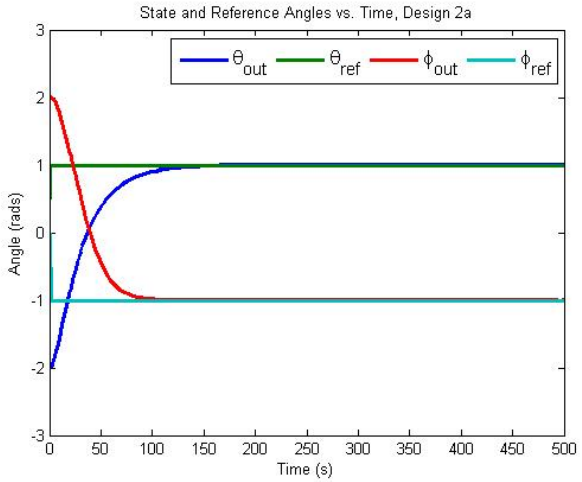

Figure 6: System response to unit-step inputs after incorporating non-linearity in input voltages, Design 2a.

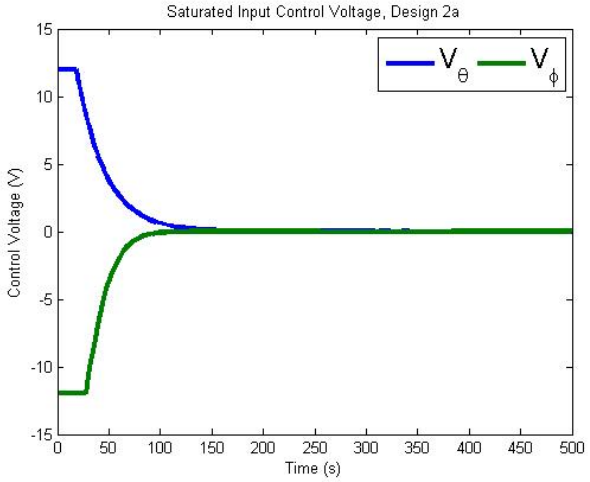

Figure 7: Plant motor voltages as a function of time for Design 2a, with plant nonlinearities. Saturation on the motor voltages V_θ and V_ϕ is clearly visible.

2) Required Controller Effort: Gain-schedulng is most interesting from the perspective of the input voltages to the motors. If we compare Figure 8 and Figure 9, we can see that the slope of V_ϕ abruptly changes at around 70 seconds, when $|\phi_{meas} - \phi|$ falls below .3 (as governed by (20)). A change in the slope of the output angle ϕ occurs in this region (see Figure 8). The same effects occur at about 85 seconds for V_θ. The slopes take on more mild climbs/descents in this region, indicating that we have met the control goal of Design 2b.

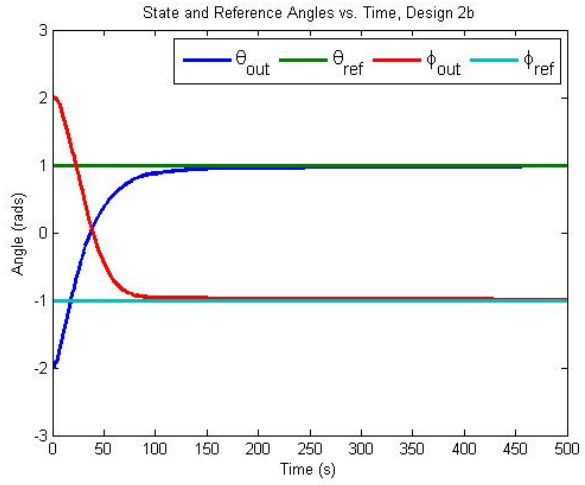

Figure 8: System response to unit-step inputs after incorporating non-linearity in plant input voltages and a gain-scheduling controller, Design 2b.

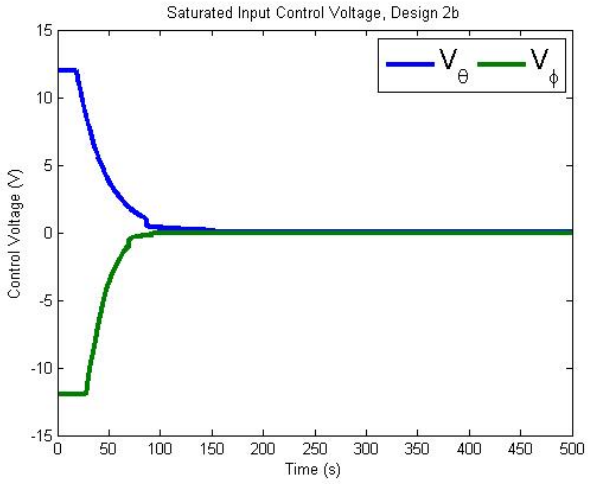

Figure 9: Plant input non-linearities, Design 2b. Input saturation of $\pm 12V$, gain-scheduled output-feedback control with K as in (20).

VIII. Discussion

For the three controlled designs discussed, different system performances were observed. State-error after 2 minutes for θ were 4.13%, 4.5%, and 8.61% for Designs 1, 2a, and 2b, respectively. State-error after 2 minutes for ϕ were .0004%, .0006%, and 2.97% for Designs 1, 2a, and 2b, respectively.

All designs met steady-state error, settling time, and overshoot requirements. Design 2a successfully implemented saturation on plant inputs, and this increased state-error after 2 minutes by .37% for θ and .0002% for ϕ from Design 1. Design 2b incorporated model non-linearities from 2a and successfully implemented gain-scheduling based on output-angle deviation from reference. This increased the state-error after two minutes by 4.48% in θ and 2.97% in ϕ from Design 1.

Control efforts varied widely based on the design chosen. Design 1 had no saturation requirement and varied by $\pm 21V$ (Figure 5). Design 2a had increased settling-time due to the saturated control effort (Figure 7). Constraints in Design 2b had the effect of increasing the settling-time even further, as we invoke less control effort during periods of small angle difference (Figure 9).

IX. Conclusions

The incorporation of saturation requirements on the inputs to a system are easy to implement after initial design work has been accomplished. For a transition from Design 1 to Design 2a, absolutely no redesign of the system was necessary. The incorporation of gain-scheduling had more startling effects in Design 2b, and if my control goals had been less lenient a complete redesign of K_0 and N_0 may have been necessary.

X. Future Work

Future topics of interest include attempting to build a controller for power output optimization. This will be implemented by means of a solar insolation sensor that determines whether it is energetically advantageous to move the photovoltaic device or keep it in its current orientation. This is applicable in areas where cloud cover would prevent large gains in solar insolation regardless of control. I would also like to physically implement and quantitatively compare the performance of non-tracking photovoltaic devices and the three reference-tracking designs I have proposed.

References

[1] Walker, Andy. *Solar Energy: Technologies and the Project Delivery Process for Buildings*. RSMeans Publishing. 2013. Print.

[2] National Renewable Energy Laboratory, "NREL: MIDC/Vehicle Testing and Integration Facility RSR", 2015. [Online]. Available: http://www.nrel.gov/midc/vtif_rsr/. [Accessed: 07- Apr- 2015].

[3] SolarWorld, "SunModule Plus SW 250 mono" SW-02-5001US datasheet, July, 2012.

[4] Motor Power Group, "Penta DC Motor" datasheet 11011300002, November, 2004.

[5] B. Messner, D. Tilbury, R. Hill and J. Taylor, "Motor Position: State-Space Methods for Controller Design", Controls Tutorials for Matlab & Simulink, 2015. [Online]. Available: http://ctms.engin.umich.edu/CTMS/index.php?example=Motor Position&section=ControlStateSpace. [Accessed: 07- Apr- 2015].

[6] K. Johnson. EENG 517. Lecture 13, Topic: "Output Feedback and Reduced Order Estimators" Faculty of Electrical Engineering, Colorado School of Mines, Golden, Colorado, Feb. 24, 2015.